Desalination and Water Treatment
www.deswater.com
doi: 10.5004/dwt.2019.23677

147 (2019) 373–384
April

The adsorption of Reactive Black 5 by nanowire-synthesized nano-manganese dioxide and nano-manganese oxyhydroxide in a natural nanoclay substrate: an adsorption kinetics and isotherm study

Shirin Delafrouz, Forogh Adhami*

Department of Chemistry, Faculty of Science Yadegar–e–Imam Khomeini (RAH) Shahre-Ray Branch, Islamic Azad University, P.O. 18155/144, Tehran, Iran, Tel. +9821 55229200; Fax: +9821 55229297; emails: fadhami@iausr.ac.ir, fadhami@gmail.com (F. Adhami), shirin.delafrouz@gmail.com (S. Delafrouz)

Received 21 January 2018; Accepted 22 December 2018

ABSTRACT

The compounds nano-manganese oxyhydroxide (γ-MnOOH) and nano-manganese dioxide (β-MnO_2) and their composites with montmorillonite (γ-MnOOH/M and β-MnO_2/M) were used for the first time to adsorb and remove the residual Reactive Black 5 (RB5) dye from textile industrial wastewater. The synthesis of γ-MnOOH and β-MnO_2 through the hydrothermal method resulted in the nanowire morphology of these compounds. Two new composites were synthesized by the interaction of these compounds with natural nanoclay montmorillonite. These compounds were able to penetrate montmorillonite nanolayers and intercalate them. The synthesized compounds and composites were characterized using Fourier-transform infrared spectroscopy, X-ray diffraction and scanning electron microscopy. The capacity of the compounds and composites to adsorb the RB5 was investigated in an artificial industrial wastewater. Both compounds and their composites were able to adsorb the dye and the results indicated the dependence of the adsorption capacity on different parameters, including pH, contact time, adsorbent dosage, and dye concentration. As expected, the composites showed a higher dye removal efficiency than the compounds, and the most sufficient dye adsorption (70%) was detected in the composite β-MnO_2/M for a dye concentration of 500 mg L^{-1}. The reusability of β-MnO_2 was also demonstrated for an efficient adsorption. The adsorption kinetics of compounds and composites followed the pseudo-second-order kinetic and the rate constants (k_2) of the compounds were higher than those of the composites. The adsorption isotherms of γ-MnOOH and β-MnO_2 corresponded to the Langmuir and Freundlich isotherms, respectively, and the adsorption isotherms of their composites followed the Langmuir isotherm. This study shows that nano-manganese compounds and their composites are efficient adsorbents for the removal of RB5 dye from industrial wastewater.

Keywords: Manganese oxyhydroxide; Manganese dioxide; Montmorillonite; Adsorption; Dye removal

1. Introduction

Different industries, such as the textile, plastic, wool, paper, cotton, food, carpet, pharmaceutical, cosmetic and silk industries, use dyes on a large scale for several applications. The residual dye in industrial wastewater has a negative impact on ecosystems [1]. Researchers have therefore sought to establish efficient procedures to remove the colored pollutants from wastewater to decrease its negative environmental effects. The textile industry has an extensive need for different dyes and is the main permanent consumer of color products [2] and thereby the main producer of colored wastewater.

Given their solubility, structure, and chemical properties, dyes are classified into different groups, such as reactive, direct, vat, basic, and acid dyes [1,3–6]. About 76% of the

* Corresponding author.

dyes discharged by the textile industries belong to the reactive (36%), acid (25%), and direct (15%) groups [7]. Due to the bright color, good solubility, and simple operation of reactive dyes, they are the most-used dye group in the textile industry. Dye removal from wastewater can be carried out by various methods such as, adsorption [8], coagulation and flocculation [9], electrocoagulation [10,11], biological methods [4,12], advanced oxidation procedures [13,14], membrane filtration [15], and reverse osmosis [16]. In practical and economic aspects, the adsorption technique has proven to be a simple and cost-effective operation for treating a high volume of wastewater [17]. Different kinds of adsorbents are used for the adsorption technique, including agricultural waste [3,18,19], industrial waste products [20,21], natural inorganic materials (bentonite) [22], sepiolite [23], vermiculite [24], gypsum [25], kaolin [26,27], zeolite [28], perlite [29], feldspar [30], activated carbon in different forms [31,32], carbon nanotube [33], alginate [34], activated sludge [35], and chemical synthetic materials [36,37].

As synthetic materials, different manganese oxides, including MnO, MnO_2, and Mn_3O_4, are often used as adsorbent [38], molecular sieve [39], and catalyst [40,41]. Among the existing manganese oxides, manganese dioxide is the most widely used with its high surface area and diverse crystal structures [42–45]. The phases, sizes, and morphologies of manganese dioxide play an important role in its properties and applications [46–48].The reported morphologies include nanotube [49], nanorod [44], nanowire [50], flower-like [51], and nanospindle [52] and phases such as "α" [36], "γ" [37], and "ε" [47].

A simple and low-cost production, efficient dye adsorption, possibility of regeneration, safe disposal without environmental damage, and potential use as a natural-based material (montmorillonite) make manganese compounds and their composites attractive candidates for the present study of dye adsorption. Considering these positive practical and economic aspects, the present research used manganese compounds (γ-MnOOH and β-MnO_2) and their montmorillonite composites (γ-MnOOH/M and β-MnO_2/M) for the first time to remove Reactive Black 5 (RB5) dye from textile industry wastewater.

2. Experimental materials and methods

2.1. Materials and instruments

$KMnO_4$, C_2H_5OH, $AgNO_3$, HCl, and cetyltrimethylammouniumbromide (CTAB) were supplied by Merck and used without further purification. Montmorillonite (CEC = 100 meq 100 g^{-1}) was purchased from Jilin Liufangzi Bentonite Science and Technology, China. Commercial anionic Reactive Black 5 (RB5) dye (Fig. 1) with color index number 20505 (molecular weight 991.82 g mol^{-1}, molar absorptivity (ε) 0.0344 L mg^{-1}, and maximum wavelength (λ_{max}) 597 nm) was supplied from Tianjin Level Chemical Company, China.

Fourier transform infrared spectra (FTIR) of the samples were recorded by the Broker, Tensor 27 spectrometer, using KBr (Mid-Infrared, 4,000–400 cm^{-1}) pellets. The phase composition and structure of samples were defined by the X-ray powder diffractometer, Philips, PW 1800(Cu Kα radiation, λ = 1.54060 Å).

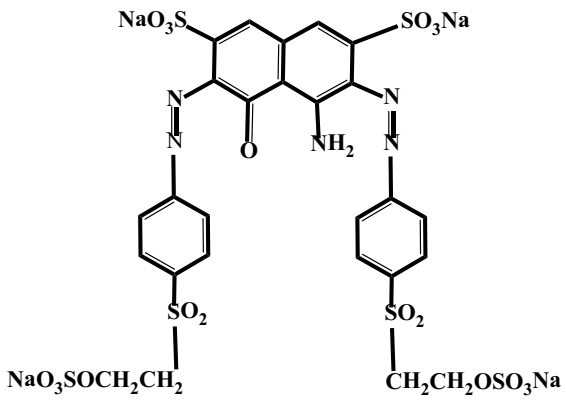

Fig. 1. Structure of RB5.

The size and surface morphologies of synthesized adsorbents were determined using the scanning electron microscopy (SEM), Philips, XL 30.

The concentration of RB5 dye was measured by ultraviolet visible spectrophotometer, Biocary, Varian 100.

2.2. Method

The nano-manganese oxyhydroxide (γ-MnOOH), nano-manganese dioxide (β-MnO_2) compounds and the nano-manganese oxyhydroxide/montmorillonite (γ-MnOOH/M) and nano-manganese dioxide/montmorillonite (β-MnO_2/M) composites were synthesized and characterized.

2.2.1. Synthesis of γ-MnOOH and β-MnO_2 compounds

The γ-MnOOH compound was synthesized using reported hydrothermal method [53] that was modified in our laboratory. $KMnO_4$ (1.5 g, 9.5 × 10^{-3} mol) was solved in 65 mL CTAB solution (1 mM), then 4 mL (0.06 mol) absolute ethanol was added and the solution was stirred at room temperature until it was precipitated and became colorless (about 45 min). This mixture was transferred to a stainless steel autoclave, which was placed in the oven at 116°C for 24 h. Mixture was cooled at room temperature and filtered. The brown precipitate (MnOOH) was washed with water and dried at 80°C for 2 h.

The MnO_2 compound was synthetized by calcination of MnOOH, at 300°C for 3 h.

2.2.2. Preparation of γ-MnOOH/M and β-MnO_2/M composites

Montmorillonite was added to 10% HCl (1:100, w/v) and the mixture was stirred for 1 h at room temperature. The mixture was filtered and the filtrate (Montmorillonite) was washed with distilled water. The washed filtrate was mixed with the appropriate compound (γ-MnOOH, β-MnO_2) (2:1 w/w) and stirred (300 rpm) for 3 h at room temperature. The mixture was filtered and the filtrate (γ-MnOOH/M, β-MnO_2/M) was washed and dried in oven at 70°C for 2 h.

2.2.3. Dye removal

Dye adsorption on the synthetized compounds and composites was studied at different conditions of pH, contact time, dye concentration and adsorbent dosage.

Dye solutions imitating textile industrial wastewater were prepared at different concentrations of dye (20, 30, 40, 50, 100, 200, 300, 500, 700, and 900 mg L^{-1}).The concentrations (mg L^{-1} deionized water) of the chemical compounds contained in the solution imitating textile industrial wastewater were as follows: sucrose ($C_{12}H_{22}O_{11}$, 600 mg L^{-1}), starch (($C_6H_{10}O_5$) *n*, 1,000 mg L^{-1}), sodium lauryl sulphate ($NaCl_{12}H_{25}SO_4$, 100 mg L^{-1}), acetic acid (CH_3COOH, 200 mg L^{-1}), sodium chloride (NaCl, 3,000 mg L^{-1}), sodium carbonate (Na_2CO_3, 500 mg L^{-1}), sodium hydroxide (NaOH, 175 mg L^{-1}), sulfuric acid (H_2SO_4, 300 mg L^{-1}) [54].

Mixtures (10 mL) of the adsorbents (at different dosages) and dye solutions (for each concentration) were prepared with different pH values (phosphate and acetate buffer solutions).These mixtures were stirred (at 120 rpm in room temperature) for defined contact times and were then immediately centrifuged. The adsorption of the supernatant (residual dye) was measured by UV–Vis spectrophotometer. The experiment was performed in triplicate.

3. Results and discussion

The synthesis of compounds and their composites were analyzed by structural and morphological characterization using FTIR spectra, X-ray diffraction (XRD) patterns and SEM images. The dye adsorption process was characterized based on defined adsorption kinetics and isotherm.

3.1. Structural and morphological characterization

The synthesis of γ-MnOOH by the reduction of $KMnO_4$ (Mn^{7+} to Mn^{3+}) and the synthesis of β-MnO_2 by the oxidation of γ-MnOOH (Mn^{3+} to Mn^{4+}) were demonstrated by structural and morphological characterization using different methods. A structural analysis was used to characterize the production of composites by the intercalation of the compounds into nanolayers.

3.1.1. FTIR spectroscopy

The absorption bands above 3,400 cm^{-1} detected in γ-MnOOH, β-MnO_2 and their composites are attributed to the O–H stretching bands. The O–H stretching band in β-MnO_2 is caused by captured water molecules. The observed absorption bands, including 596 and 490 cm^{-1} in γ-MnOOH, 519 cm^{-1} in β-MnO_2, 594 and 522 cm^{-1} in γ-MnOOH/M and 527 cm^{-1} in β-MnO_2/M indicate the stretching of Mn–O bond in these products [51,55].

The broad band at 1,036–1,039 cm^{-1} detected in the composites confirms the stretching of Si–O bond in montmorillonite. The detected absorption bands, including 522 and 452 cm^{-1} in γ-MnOOH/M and 527 and 465 cm^{-1} in β-MnO_2/M are related to the Si–O–Si bending in montmorillonite [56].Some absorption bands of γ-MnOOH, β-MnO_2 and montmorillonite overlap in their composites.

3.1.2. X-Ray diffraction

The XRD patterns of γ-MnOOH, β-MnO_2, montmorillonite, γ-MnOOH/M and β-MnO_2/M are shown in Fig. 2. The pattern of γ-MnOOH confirms the γ-phase (nine peaks with miller indices (111), (020), (002), (121), (012), (113), (131), (202), and (222), JCPDS NO: 00-041-1379, Fig. 2(a)) [42]. The pattern of β-MnO_2 confirms the β-phase (six peaks with miller indices (110), (101), (111), (211), (220), and (002), JCPDS NO: 00-024-0735, Fig. 2(b)) [57,58]. The patterns of γ-MnOOH and β-MnO_2 are not changed in the composites and their crystalline structures remain stable.

The pattern of montmorillonite shows a peak at 2θ = 6.76 (*d* = 1.305 nm, Fig. 2(c)), which is changed similarly in both composites as a result of the intercalation of montmorillonite [59] by γ-MnOOH and β-MnO_2.This peak is changed to 2θ = 6.28 (*d* = 1.405 nm) in γ-MnOOH/M composite (Fig. 2(d)) and to 2θ = 6.29 (*d* = 1.401 nm) in β-MnO_2/M composite (Fig. 2(e)).

3.1.3. Scanning electron microscopy

SEM images of γ-MnOOH (Fig. 3(a)) and β-MnO_2 (Fig. 3(b)) indicate the similar nanowire morphologies (diameter ~ 36 nm, length ~ 1,000 nm) for both compounds. As shown in Fig. 3(c) and (d), the nanolayer morphology of montmorillonite is not changed by the intercalation of the compounds into the montmorillonite.

3.2. Dye adsorption process

The adsorption of RB5 by γ-MnOOH, β-MnO_2, γ-MnOOH/M, and β-MnO_2/M was investigated under different pH values, contact times, amounts of adsorbent and dye concentrations for optimizing the dye removal conditions. Dye adsorption on β-MnO_2, γ-MnOOH/M, and β-MnO_2/M is based on electrostatic interactions, and dye adsorption on γ-MnOOH is caused by the hydrogen bonds formed between γ-MnOOH (oxygen atoms and OH groups) and the dye molecules. The dye concentration (c_t), calculated by UV–Vis spectrophotometry [60], was used to define the adsorption kinetics and isotherms.

3.2.1. pH

pH is an important parameter in the adsorption process that affects the adsorbent capacity, dye solubility, and surface of the adsorbent [19]. Dye adsorption was therefore investigated at different pH values, including 4, 7, and 10 (Fig. 4).The highest adsorption capacity for γ-MnOOH was observed at the pH of 10, which increased the hydrogen bonds between the dye molecules and the compound. Through the hydrogen bondings, the OH^- ions that are connected to the positive hydrogens on the surface of γ-MnOOH (Fig. 5) attach to the negatively-charged RB5 dye molecules [2]. β-MnO_2, β-MnO_2/M ,and γ-MnOOH/M showed the highest adsorption capacity at the lowest pH value, resulting in an increase of the electrostatic attraction between the dye molecules and the compound/composites. Through the electrostatic attractions, the H^+ ions act as a bridge between the negatively-charged surfaces of β-MnO_2 (Fig. 5) and the nanolayers of montmorillonite and the anionic dye molecules.

3.2.2. Contact time

The contact time between the adsorbate and the adsorbent is a significant parameter in the adsorption process. At the

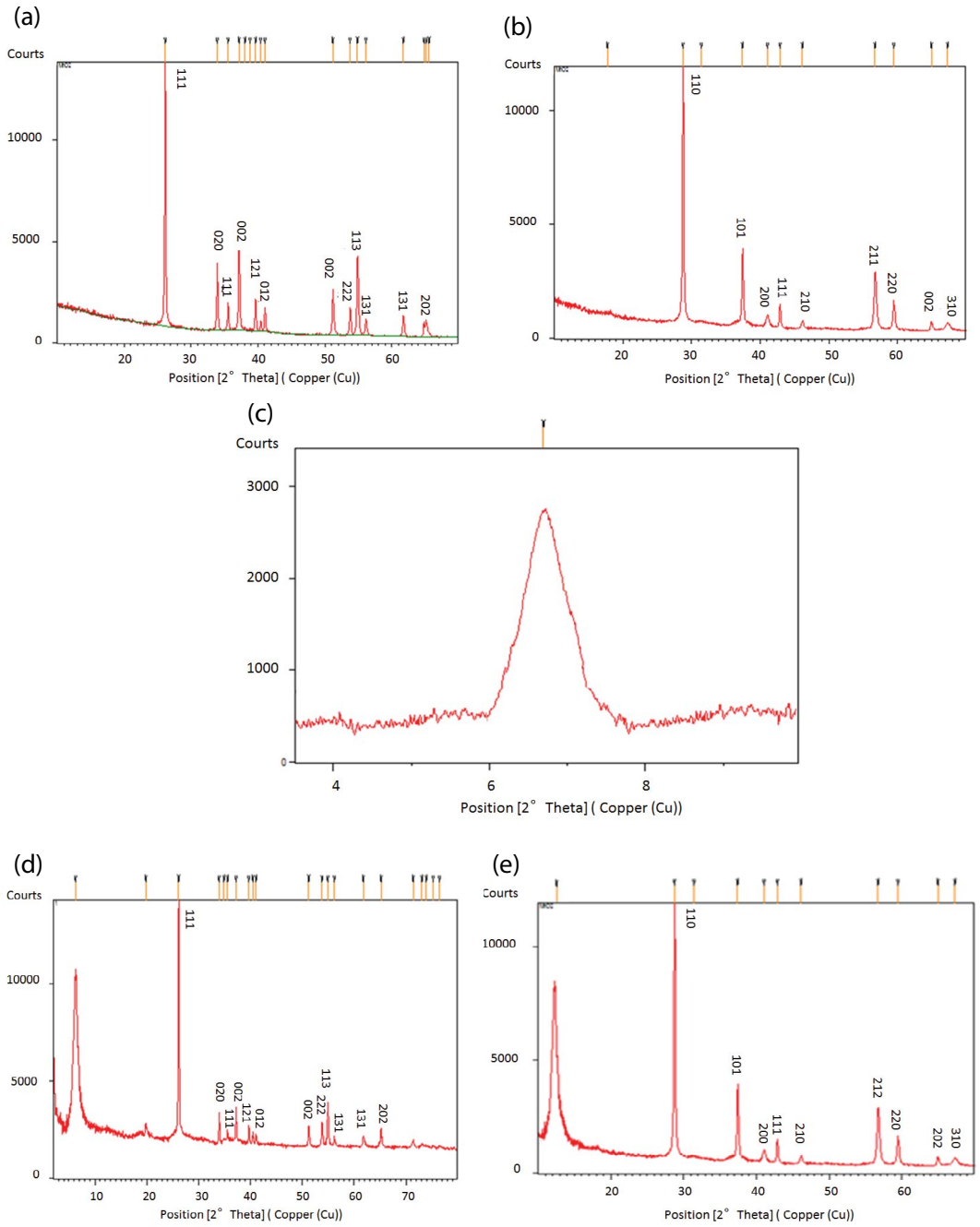

Fig. 2. XRD patterns of, (a) γ-MnOOH, (b) β-MnO_2, (c) montmorillonite, (d) γ-MnOOH/M, and (e) β-MnO_2/M.

optimized pH value, maximum adsorption was achieved after 45 min for both compounds, where γ-MnOOH showed the higher adsorption. For γ-MnOOH/M and β-MnO_2/M, the maximum adsorption was reached after 90 and 120 min, respectively, and β-MnO_2/M showed the higher adsorption. Considering the montmorillonite nanolayer structure, the composites needed a longer contact time to reach the maximum adsorption (Fig. 6).

3.2.3. Adsorbent dosage

The adsorption capacity was analyzed at the optimized pH and contact time under different adsorbent dosages. The maximum adsorption of the compounds was observed at 1 g L^{-1} and γ-MnOOH had the higher adsorption. The composites showed a maximum adsorption at 2 g L^{-1} and the adsorption of β-MnO_2/M was higher. γ-MnOOH showed the highest adsorption with a dosage of 1 g L^{-1} (Fig. 7).

3.2.4. Dye concentration

The adsorption capacity was investigated by different dye concentrations (20–900 mg L^{-1}) at optimized pH, contact time and adsorbent dosage conditions. At low dye concentrations (20–40 mg L^{-1}), γ-MnOOH showed the highest adsorption

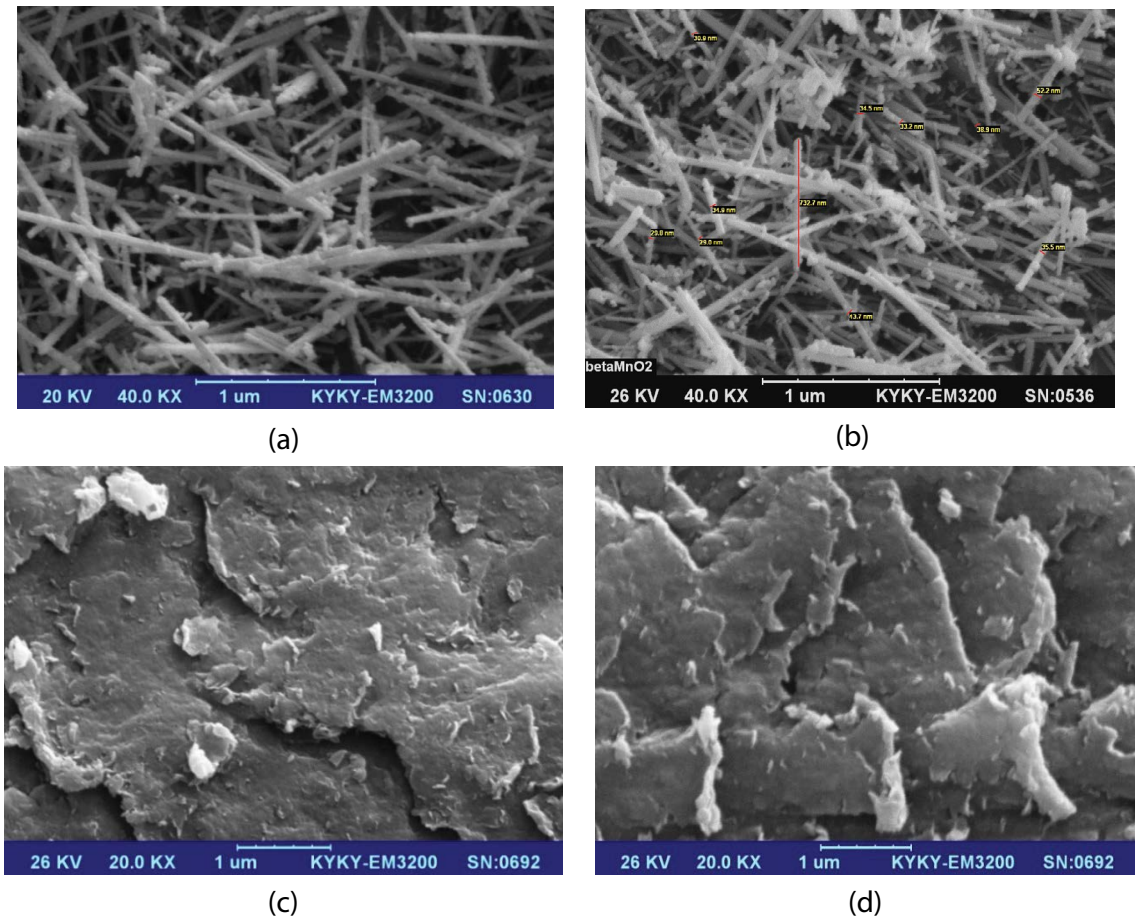

Fig. 3. SEM patterns of, (a) γ-MnOOH, (b) β-MnO_2 (~36 and 1,000 nm, diameter and length), (c) montmorillonite, and (d) γ-MnOOH/M.

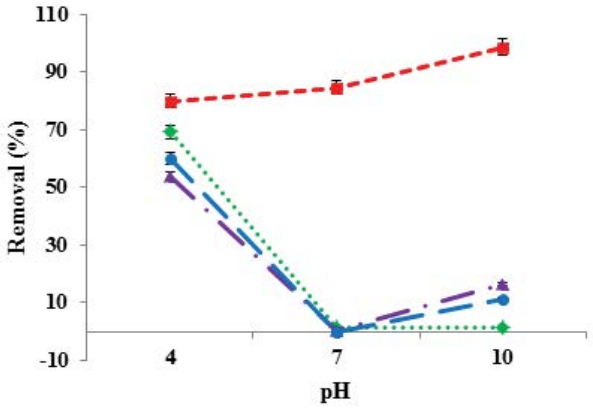

Fig. 4. Effect of pH on RB5 adsorption (Adsorbent = 1 g L^{-1}, Time = 45 min, [dye] = 30 mg L^{-1}) γ-MnOOH (■, SD = ± 2.70%), β-MnO_2 (◆, SD = ± 3.30%) γ-MnOOH/M (▲, SD = ± 3.10%), β-MnO_2/M (●, SD = ± 3.60%).

(~100%), which could be related to the hydroxyl groups on the surface of γ-MnOOH, which increase the hydrogen bonds. At high dye concentrations, the most efficient dye removal was 70% for β-MnO_2/M (500 mg L^{-1}), followed by 60% for γ-MnOOH/M (300 mg L^{-1}), 67% for γ-MnOOH (100 mg L^{-1}) and 63% for β-MnO_2 (200 mg L^{-1}).The β-MnO_2/M composite showed the most significant dye adsorption of 70% with a concentration of 500 mg L^{-1} (Fig. 8).

Table 1 presents a summary of the results obtained for adsorption at different conditions. As shown, the β-MnO_2/M composite is the most efficient adsorbent.

3.3. Reusability

There generation and reusability of adsorbents has economic relevance. Washing or heating are two main procedures used to remove dyes and regenerate adsorbents [63,64]. Adsorbents are regenerated without any chemical changes and can be released without any negative environmental impact. Due to cost issues, the washing technique was used for regenerating the adsorbent β-MnO_2. A mixture of adsorbent (β-MnO_2, 0.01 g) and dye (50 mg L^{-1}, pH = 4) was prepared, stirred for 45 min and then centrifuged. The filtrate (β-MnO_2 + dye) was washed (in 3 mL of water)and centrifuged to remove the dye and regenerate the adsorbent. The filtrate (regenerated β-MnO_2) was used again for dye adsorption under the same conditions. This process was repeated seven times. The adsorption capacity of 72%, reached in the first adsorption cycle, was reduced to 60% in the seventh cycle. This small reduction in adsorption

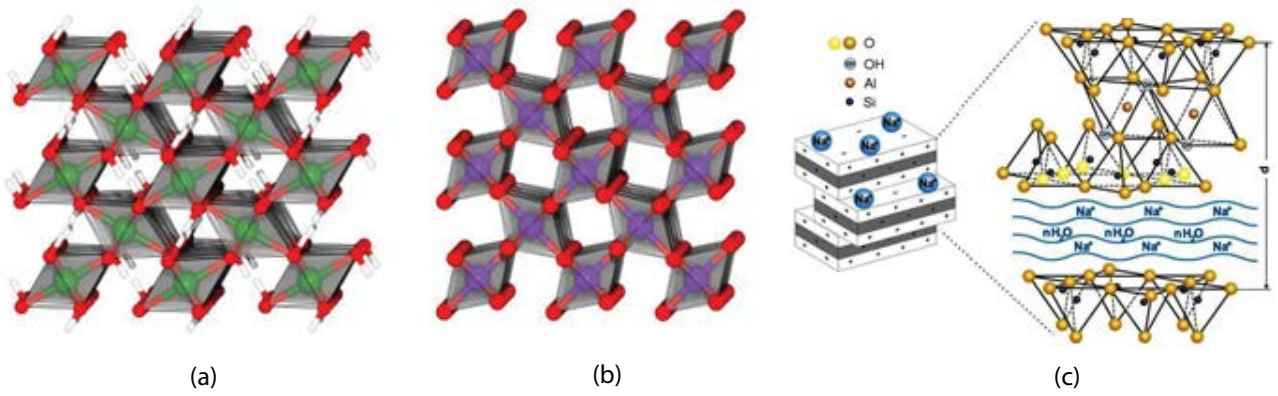

Fig. 5. Scheme of the structures of (a) γ-MnOOH [61], (b) β-MnO_2 [61], and (c) montmorillonite [62].

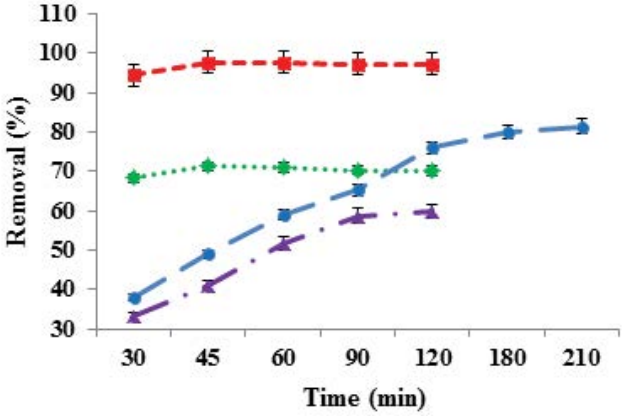

Fig. 6. Effect of contact time on RB5 adsorption (Adsorbent = 1 g L^{-1}, [dye] = 30 mg L^{-1}), γ-MnOOH (■, SD = ± 2.80%) pH = 10, β-MnO_2 (♦, SD = ± 1.70%) pH = 4, γ-MnOOH/M (▲, SD = ± 3.10%) pH = 4, β-MnO_2/M (●, SD = ± 2.20%) pH = 4.

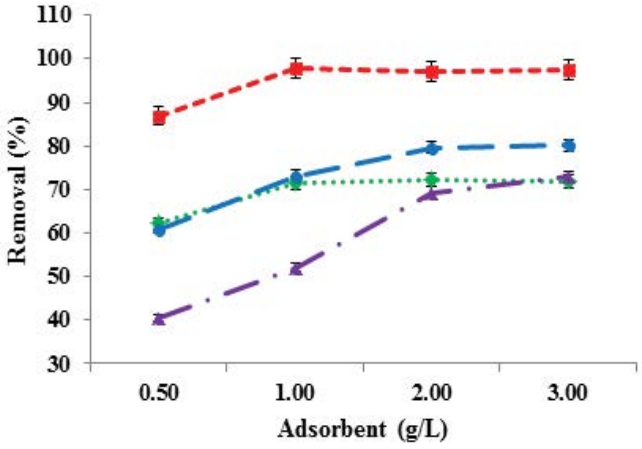

Fig. 7. Effect of adsorbent dosage on RB5 adsorption, [dye] = 30 mg L^{-1}, γ-MnOOH (■, SD = ± 2.35%) pH = 10, Time = 45 min, β-MnO_2 (♦, SD = ± 2.20%) pH = 4, Time = 45 min, γ-MnOOH/M (▲, SD = ± 1.90%) pH = 4, Time = 90 min, β-MnO_2/M (●, SD = ± 1.70%) pH = 4, Time = 120 min.

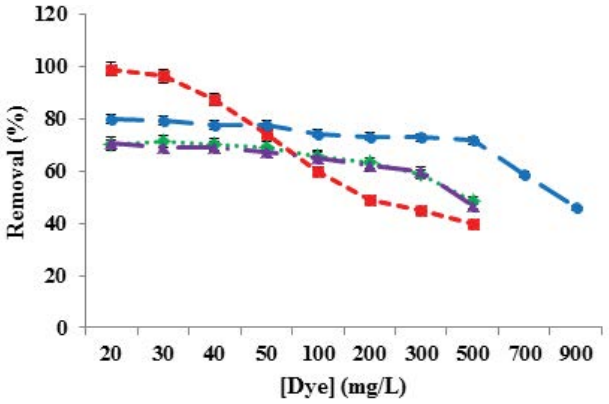

Fig. 8. Effect of initial dye concentration on RB5, adsorption γ-MnOOH (■, SD = ± 2.75%) Adsorbent = 1 g L^{-1}, pH = 10, Time = 45 min, β-MnO_2 (♦, SD = ± 3.20%) Adsorbent = 1 g L^{-1}, pH = 4, Time = 45 min, γ-MnOOH/M (▲, SD = ± 2.98%) Adsorbent = 2 g L^{-1}, pH = 4, Time = 90 min, β-MnO_2/M (●, SD = ± 2.15%) Adsorbent = 2 g L^{-1}, pH = 4, Time = 120 min.

Table 1
Best condition on removal of RB5 by γ-MnOOH, β-MnO_2, γ-MnOOH/M, β-MnO_2/M, and M

Sample	pH	Time (min)	Adsorbent (g L^{-1})	[Dye] (mg L^{-1})	*R*(%)
γ-MnOOH	10	45	1	100	67.51
β-MnO_2	4	45	1	200	63.14
γ-MnOOH/M	4	90	2	300	59.79
β-MnO_2/M	4	120	2	500	71.72
M	4	90	2	100	< 20

capacity demonstrates the efficiency of regenerating and reusing β-MnO_2 (Fig. 9).

3.4. Adsorption kinetics and isotherms

3.4.1. Kinetics study

Adsorption kinetics study was performed for the compounds γ-MnOOH and β-MnO_2 and the composites

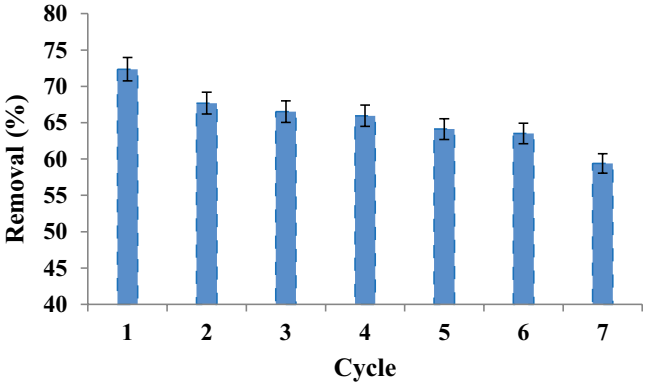

Fig. 9. Reusability of β-MnO_2 on RB5 adsorption, Adsorbent = 1 g L^{-1}, pH = 4, Time = 45 min, [dye] = 50 mg L^{-1} (SD = ± 2.25%).

γ-MnOOH/M and β-MnO_2/M at a dye concentration of 30 mg L^{-1}. The pseudo-first-order kinetic model (Lagergren, 1898, Eq. (1)) [65] as well as the pseudo-second-order kinetic model (Ho and McKay, 1998, Eq. (2)) [55,65] were applied to define the adsorption kinetics.

$$\log\left(q_{eq}-q_t\right)=\log q_{eq}-\left(\frac{k_1}{2.303}\right)t \quad (1)$$

$$\frac{t}{q_t}=\frac{1}{\left(k_2 q_{eq}^2\right)}+\left(\frac{1}{q_{eq}}\right)t \quad (2)$$

As demonstrated in Fig. 10, the adsorption kinetics of all the compounds and composites followed the pseudo-second-order kinetic model. The kinetic parameters, i.e. k_2 (rate constant) and q_{eq}, were higher in the compounds than in the composites, and γ-MnOOH showed the highest values (Table 2).

3.4.2. Isotherm study

The most-used adsorption isotherms, i.e. Freundlich (Eqs. (3) and (4)) and Langmuir (Eqs. (5)–(7)) [66,67], were applied to determine the adsorption isotherm for the compounds and the composites by different dye concentrations (20–900 mg L^{-1}) at optimized conditions.

$$q_e=K_f C_e^{1/n} \quad (3)$$

$$\log q_e=\log K_f+\frac{1}{n}\log C_e \quad (4)$$

$$q_e=\frac{\left(q_m b C_{eq}\right)}{\left(1+bC_e\right)} \quad (5)$$

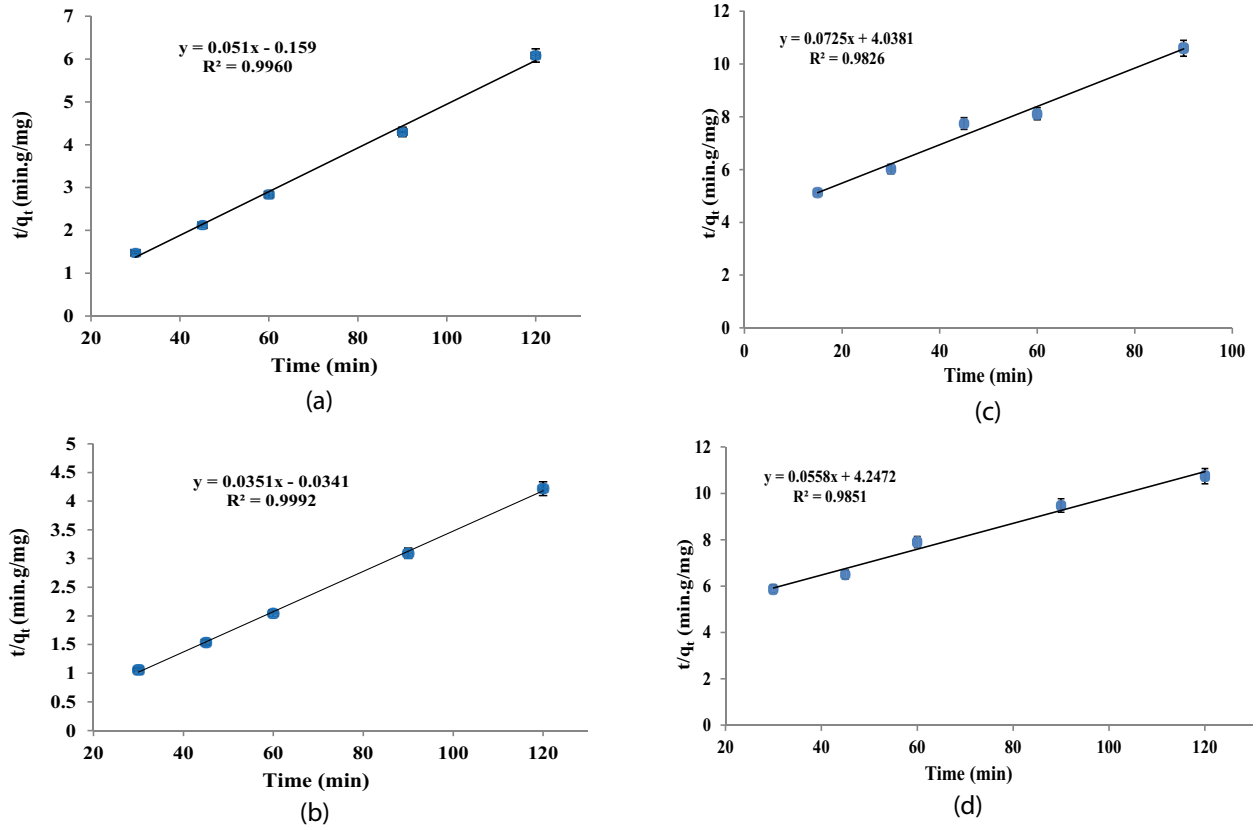

Fig. 10. Pseudo-second-order kinetic model of RB5, (a) γ-MnOOH (1 g L^{-1}, pH = 10, [dye] = 30 mg L^{-1}, SD = ± 2.85%), (b) β-MnO_2 (1 g L^{-1}, pH = 4, [dye] = 30 mg L^{-1}, SD = ± 2.54%), (c) γ-MnOOH/M (2 g L^{-1}, pH = 4, [dye] = 30 mg L^{-1}, SD = ± 2.85%), and (d) β-MnO_2/M (2 g L^{-1}, pH = 4, [dye] = 30 mg L^{-1}, SD = ± 3.05%).

Table 2
Results of the kinetics calculations of γ-MnOOH and β-MnO_2

Adsorbent	Conc. (mg L^{-1})	Pseudo-first-order kinetic			Pseudo-second-order kinetic		
		q_{eq} (mg g^{-1})	k_1 (1 min^{-1})	R^2	q_{qe} (mg g^{-1})	k_2 (g mg^{-1} min)	R^2
γ-MnOOH	30	29.509	15.660	0.924	28.490	3.612	0.999
β-MnO_2	30	24.888	15.660	0.910	19.608	1.635	0.996
γ-MnOOH/M	30	17.386	0.0490	0.945	13.793	0.0013	0.983
β-MnO_2/M	30	118.17	0.0108	0.974	17.921	0.0007	0.985

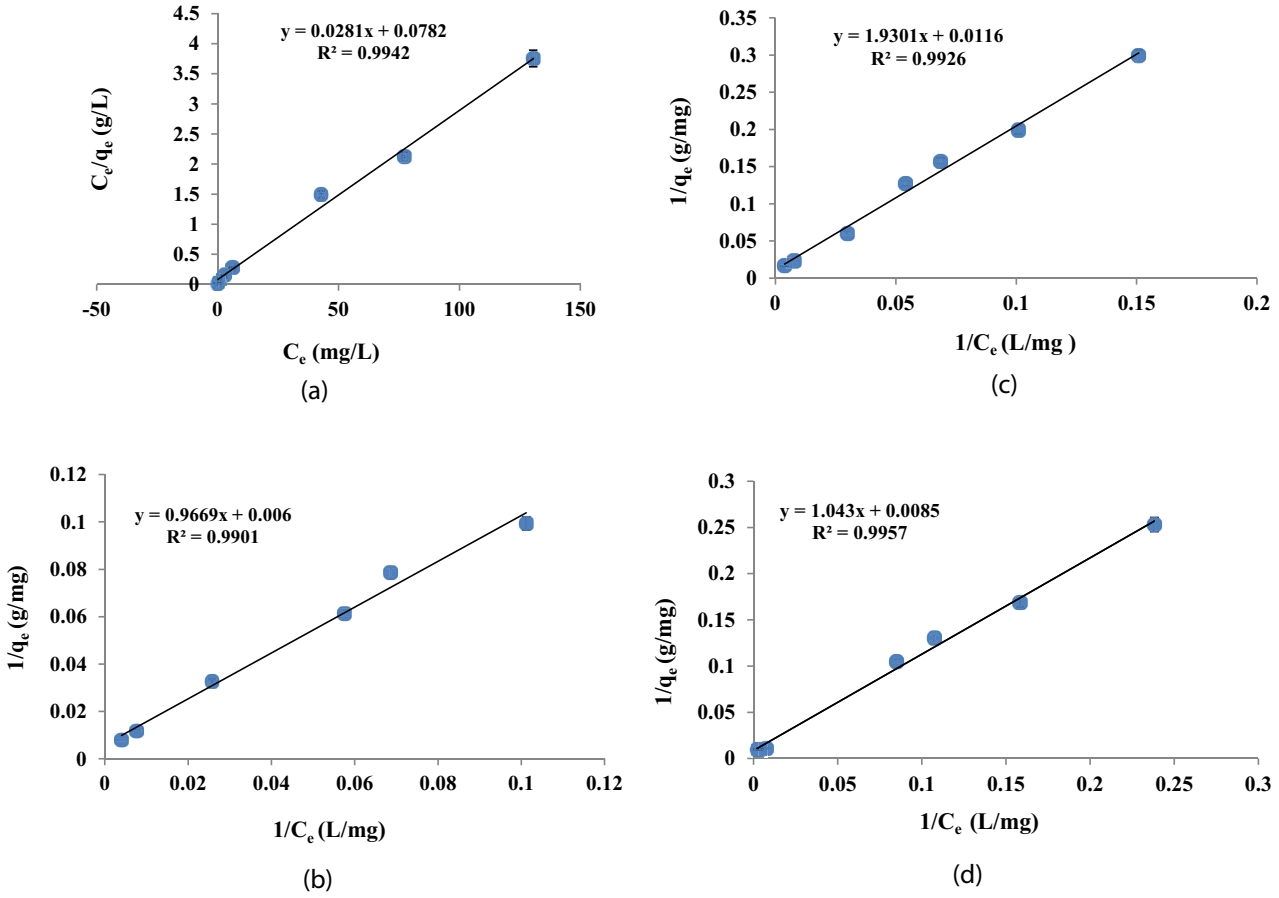

Fig. 11. Langmuir adsorption isotherms of RB5, (a) γ-MnOOH (Adsorbent = 1 g L^{-1}, pH = 10, Time = 45) (SD = ± 2.85%), (b) β-MnO_2 (Adsorbent = 1g L^{-1}, pH = 4, Time = 45) (SD = ± 3.40%), (c) γ-MnOOH/M (Adsorbent = 2 g L^{-1}, pH = 4, Time = 90) (SD = ± 3.15%), and (d) β-MnO_2/M (Adsorbent = 2 g L^{-1}, pH = 4, Time = 120) (SD = ± 2.45%).

$$\frac{C}{q_e} = \frac{C_{eq}}{q_m} + \frac{1}{(q_m b)} \tag{6}$$

$$\frac{1}{q_e} = \frac{1}{q_m} + \frac{1}{(q_m b C_e)} \tag{7}$$

The correlation coefficients (R^2) of Freundlich and Langmuir isotherms were set for all the compounds and composites. With the set R^2, γ-MnOOH and both composites follow the Langmuir isotherm, and β-MnO_2 follows the Freundlich isotherm (Figs. 11 and 12, Table 3). Since the value of all R^2s were high and close to each other, the isotherm parameters, including Freundlich isotherm constant (K_f($mg^{1-1/n}$ $L^{1/n}$ g^{-1}), adsorption intensity (n), Langmuir isotherm constant (b (L mg^{-1})) and maximum monolayer capacity (q_m (mg g^{-1})) were determined. The isotherm parameters were similar for all the adsorbents, except for γ-MnOOH.

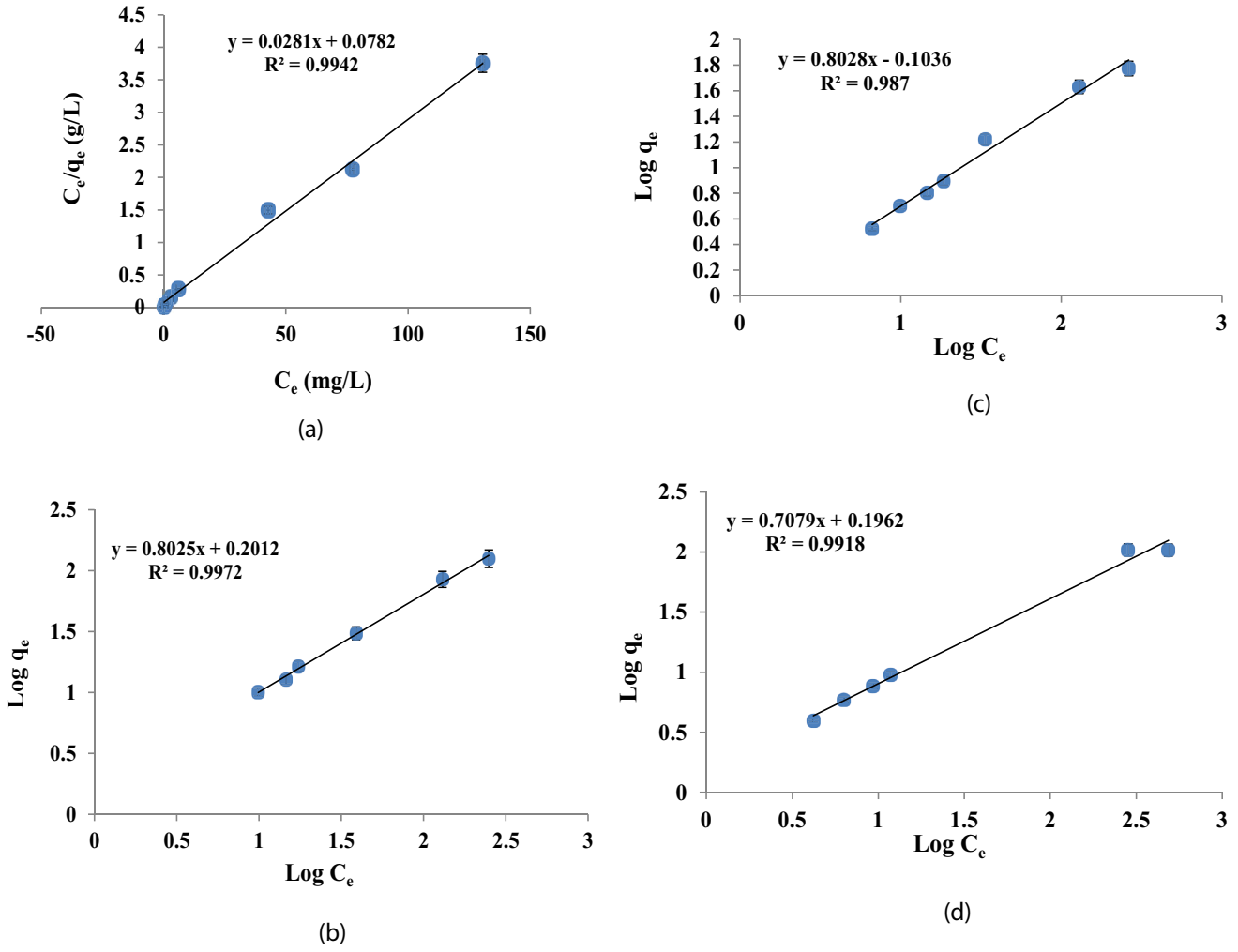

Fig. 12. Freundlich adsorption isotherms of RB5, (a) γ-MnOOH (Adsorbent = 1 g L^{-1}, pH = 10, Time = 45) (SD = ± 2.85%), (b) β-MnO_2 (Adsorbent = 1g L^{-1}, pH = 4, Time = 45) (SD = ± 3.40%), (c) γ-MnOOH/M (Adsorbent = 2g L^{-1}, pH = 4, Time = 90) (SD = ± 3.15%), and (d) β-MnO_2/M (Adsorbent = 2 g L^{-1}, pH = 4, Time = 120) (SD = ± 2.45%).

Table 3
Results of the isotherms calculations at optimum condition

Isotherm	Isotherm parameters	Adsorbent			
		γ-MnOOH	β-MnO_2	γ-MnOOH/M	β-MnO_2/M
Langmuir	b (L mg^{-1})	0.3593	0.0062	0.0046	0.0081
	q_m (mg g^{-1})	35.5872	166.6666	109.8901	117.6470
	R^2	0.9942	0.9901	0.9926	0.9957
	R_L (min)*	0.1221	0.3283	0.9157	0.8605
	R_L (max)*	0.0137	0.2439	0.3030	0.1206
Freundlich	K_f ($mg^{1-1/n}$ $L^{1/n}$ g^{-1})	14.9830	1.5892	1.2694	1.5711
	n	5.2465	1.2461	1.2456	1.4126
	R^2	0.9855	0.9972	0.9870	0.9918

Min (minimum) & max (maximum) concentrations of dye

Table 4
Adsorption capacities of different adsorbents for the RB5 adsorption (Langmuir adsorption isotherm)

Adsorbents	q_{max} (mg g^{-1})	References
Chitosan flakes	480	[68]
Chitosan beads	400	[68]
Eucalyptusbark/magnetite composite	370.7	[69]
Cetyltrimethylammonium bromide-coated magnetite	312.5	[70]
β-MnO_2	166.66	This study
Ionic liquid grafted-magnetic nanoparticles	161.29	[71]
Chitosan-intercalated montmorillonite	138.89	[4]
Chitin	130	[68]
β-MnO_2/Montmorillonite(β-MnO_2/M)	117.65	This study
γ-MnOOH/Montmorillonite (γ-MnOOH/M)	109.89	This study
Surfactant-modified activated carbon	100	[72]
Powdered activated carbon	58.823	[73]
Banana peel powder	49.2	[63]
Silica–alumina oxide	47.10	[74]
γ-MnOOH	35.58	This study
Chitosan 10B	34.197	[75]
Bentonite clay	34.01	[22]
ZnO–Fe_3O_4	22.1	[76]
Activated carbon from walnut wood	19.34	[77]
Surfactant-Modified zeolite	12.929	[78]
Cu–Cu_2O-based char	6.06	[79]
F_3O_4-based char	2.88	[79]

The equilibrium parameter of the Langmuir isotherm (R_L) was calculated for γ-MnOOH, β-MnO_2, γ-MnOOH/M, and β-MnO_2/M at respective minimum and maximum dye concentrations [64]. As expected, the values of all the R_Ls were less than 1, and γ-MnOOH showed the lowest value (Table 3).

Since most of the adsorbents used in this study follow the Langmuir isotherm, Table 4 presents an overview of the q_m values of these and other reported adsorbents (natural minerals, synthetic compounds and vegetable/fruit waste).

In addition to the q_m parameter, further factors, such as dye adsorption conditions, availability and production of adsorbent, should be considered for selecting the most efficient adsorbent.

4. Conclusion

In the course of this study, the manganese compounds γ-MnOOH and β-MnO_2, with similar nanowire morphologies, were synthesized. These compounds intercalated the nanolayers of montmorillonite and produced their respective composites, i.e. γ-MnOOH/M and β-MnO_2/M. Both compounds and composites were able to adsorb RB5 in dye solutions imitating textile industrial wastewater. At similar conditions, the highest adsorption was observed at pH = 4 for β-MnO_2 and both composites. Meanwhile, γ-MnOOH showed the best adsorption at pH = 10. At optimized pH values, the composites needed a longer contact time for an efficient adsorption. At optimized pH values and contact times, the compounds showed the lowest adsorbent dosage for the most efficient adsorption. At optimized pH values, contact times and adsorbent dosages, the highest adsorption was detected in a low dye concentration for γ-MnOOH and in a high dye concentration for β-MnO_2/M. The most adequate dye adsorption (70%) was detected for the composite β-MnO_2/M by a dye concentration of 500 mg L^{-1}. The regeneration experiment showed that β-MnO_2 is a reusable adsorbent with a high adsorption capacity.

The adsorption kinetics of compounds and composites thus follow the pseudo-second-order kinetic model. The k_2 and q_{eq} of compounds were higher than those of the composites, and γ-MnOOH showed the highest value.

The results obtained for the adsorption isotherms showed that γ-MnOOH and the composites follow the Langmuir isotherm and β-MnO_2 follows the Freundlich isotherm.

All the adsorbents, except for γ-MnOOH, showed similar values for the Freundlich and Langmuir isotherm parameters K_f, n, b, and q_m.

Based on the present finding, manganese compounds (γ-MnOOH and β-MnO_2) and their composites (γ-MnOOH/M and β-MnO_2/M) have proven to be suitable adsorbents for removing different concentrations of RB5 dye from textile industrial wastewater. Their relatively low cost, simple production steps, and possibility of reuse make these materials good candidates for use as efficient dye adsorbents for the treatment of industrial wastewater.

Acknowledgment

We are grateful to the Islamic Azad University, Yadegar–e–Imam, Shahre–Ray Branch for their support.

References

[1] M. Arami, N.Y. Limaee, N.M. Mahmoodi, N. Salman Tabrizi, Removal of dyes from colored textile wastewater by orange peel adsorbent: equilibrium and kinetic studies, J. Colloid Interface Sci., 288 (2005) 371–376.

[2] K. Suganya, K. Revathi, Decolorization of reactive dyes by immobilized bacterial cells from textile effluents, Int. J. Curr. Microbiol. Appl. Sci., 5 (2016) 528–532.

[3] H. Ucun, Equilibrium, thermodynamic and kinetics of Reactive Black 5 biosorption on loquat seed, Sci. Res. Essays, 6 (2011) 4113–4124.

[4] C. Umpuch, S. Sakaew, Adsorption characteristics of Reactive Black 5 onto chitosan-intercalated monmorillonite, Desalin. Water Treat., 53 (2015) 2962–2969.

[5] M. Šmelcerović, D. Đordević, M. Novaković, M. Mizdraković, Decolorization of a textile vat dye by adsorption on waste ash, J. Serb. Chem. Soc., 75 (2010) 855–872.

[6] N.M. Mahmoodi, A. Dalvand, Treatment of colored textile wastewater containing acid dye using electrocoagulation process, Desalin. Water Treat., 51 (2013) 5959–5964.

[7] M.P. Shah, K.A. Patel, Microbial degradation of Reactive Red 195 by three bacterial isolates in anaerobic-aerobic bioprocess, Int. J. Environ. Bioremediat. Biodegrad., 2 (2014) 5–11.

[8] T.W. Seow, C.K. Lim, Removal of dye by adsorption: a review, IJAER, 11 (2016) 2675–2679.

[9] K. Singh, S. Arora, Removal of synthetic textile dyes from wastewaters: a critical review on present treatment technologies, Crit. Rev. Env. Sci. Technol., 41 (2011) 807–878.

[10] B. Khemila, B. Merzouk, A. Chouder, R. Zidelkhir, J.P. Leclerc, F. Lapicque, Removal of a textile dye using photovoltaic electrocoagulation, Sustain. Chem. Pharm., 7 (2018) 27–35.

[11] N.M.A. Ghalwa, A.M. Saqer, N.B. Farhat, Removal of Reactive Red 24 dye by clean electrocoagulation process using iron and aluminum electrodes, J. Chem. Eng. Process Technol., 7 (2016) 1–7.

[12] Archna, K.N. Lokesh, R.R.S. Kiran, Biological methods of dye removal from textile effluents – a review, J. Biochem. Technol., 3 (2012) S177–S180.

[13] M. Shaban, M.R. Abukhadra, S.S. Ibrahim, M.G. Shahien, Photocatalytic degradation and photo-fentonoxidation of Congo Red dye pollutants in water using natural chromite-response surface optimization, Appl. Water Sci., 7 (2017) 4743–4756.

[14] V. Vaiano, G. Iervolino, L. Rizzo, D. Sannino, Advanced oxidation processes for the removal of food dyes in wastewater, Curr. Org. Chem., 21 (2017) 1068–1073.

[15] X. Zhu, Y. Zheng, Z. Chen, Q. Chen, B. Gao, S. Yu, Removal of reactive dye from textile effluent through submerged filtration using hollow fiber composite nanofiltration membrane, Desalin. Water Treat., 51 (2013) 6101–6109.

[16] M.F. Abid, M.A. Zablouk, A.M. Abid-Alameer, Experimental study of dye removal from industrial wastewater by membrane technologies of reverse osmosis and nanofiltration, Iranian J. Environ. Health Sci. Eng., 9 (2012) 2–9.

[17] W.S. Wan Ngah, M.A.K.M. Hanafiah, Removal of heavy metal ions from wastewater by chemically modified plant wastes as adsorbents: a review, Bioresour. Technol., 99 (2008) 3935–3948.

[18] B. Ramaraju, P.M.K. Reddy, C. Subrahmanyam, Low cost adsorbents from agricultural waste for removal of dyes, Environ. Prog. Sustain. Energy, 33 (2014) 38–46.

[19] S. De Gisi, G. Lofrano, M. Grassi, M. Notarnicola, Characteristics and adsorption capacities of low-cost sorbents for wastewater treatment: a review, Sustain. Mater.Technol., 9 (2016) 10–40.

[20] M.K. Sahu, R.K. Patel, Removal of safranin-O dye from aqueous solution using modified red mud: kinetics and equilibrium studies, RSC Adv., 5 (2015) 78491–78501.

[21] C.P.C. de Jesus, M.L.P. Antunes, F.T. daconceição, G.R.B. Navarro, R.B. Moruzzi, Removal of reactive dye from aqueous solution using thermally treated red mud, Desalin. Water Treat., 55 (2015) 1040–1047.

[22] M.T. Amin, A.A. Alazba, M. Shafiq, Adsorptive removal of Reactive Black 5 from wastewater using bentonite clay: isotherms, kinetics and thermodynamics, Sustainability, 7 (2015) 15302–15318.

[23] O. Duman, S. Tunç, T.G. Polat, Adsorptive removal of triarylmetane dye (Basic Red 9) from aqueous solution by sepiolite as effective and low-cost adsorbent, Microporous. Mesoporous. Mater., 210 (2015) 176–184.

[24] O. Duman, S. Tunç, T.G. Polat, Determination of adsorptive properties of expanded vermiculite for the removal of C. I. Basic Red 9 from aqueous solution: kinetic, isotherm and thermodynamic study, Appl. Clay Sci., 109–110 (2015) 22–32.

[25] C.C. Obunwo, I. Ubong, G.I. Ordu, Removal of Reactive Red 1 dye from aqueous solution using gypsum, Int. J. Biol. Chem. Sci., 6 (2012) 2202–2210.

[26] O.T. Ogunmodede, A.A. Ojo, E. Adewole, O.L. Adebayo, Adsorptive of anionic dye from aqueous solutions by mixture of kaolin and bentonite clay: characteristics, isotherm, kinetic and thermodynamic studies, IJEE, 6 (2015) 147–153.

[27] B. Meroufel, O. Benali, M. Benyahia, Y. Benmoussa, M.A. Zenasni, Adsorptive removal of anionic dye from aqueous solutions by algerian kaoline: characteristics, isotherm, kinetic and thermodynamic studies, J. Mater. Environ. Sci., 4 (2013) 482–491.

[28] S. Syafalni, S.R.B. Sing, M.H. Zawawi, Sorption of dye wastewater by using natural zeolite, anionic-cationic surfactant modified zeolite and cationic surfactant modified zeolite, World Appl. Sci. J., 32 (2014) 818–824.

[29] W. Luo, Q. Gao, X. Wu, C. Zhou, Removal of cationic dye (Methylene Blue) from aqueous solution by humic acid-modified expanded perlite: experiment and theory, Sep. Sci. Technol., 49 (2014) 2400–2411.

[30] H.A. Awala, M.M. El Jamal, Equilibrium and kinetics study of adsorption of some dyes onto feldespar, Univ. Chem. Technol. Metall., 46 (2011) 45–52

[31] J.B. Nasr, N. Hamdi, F. Elhalouani, Characterization of activated carbon prepared from sludge paper for methylene blue adsorption, J. Mater. Environ. Sci., 8 (2017) 1960–1967.

[32] E. Ayranci, O. Duman, In-situ UV-Visible spectroscopic study on the adsorption of some dyes onto activated carbon cloth, Sep. Sci. Technol., 44 (2009) 3735–3752.

[33] O. Duman, S. Tunç, T.G. Polat, B.K. Bozoğlan, Synthesis of magnetic oxidized multiwalled carbon nanotube-κ-carrageenan-Fe_3O_4 nanocomposite adsorbent and its application in cationic Methylene Blue dye adsorption, Carbohydr. Polym., 147 (2016) 79–88.

[34] G. Vijayaraghavan, S. Shanthakumar, Removal of sulphur-black dye from its aqueous solution using alginate from *Sargassum Sp*. (Brown Algae) as a coagulant environmental progress and sustainable energy, Global NEST J., 34 (2015) 1427–1434.

[35] H.C. Chu, L.H. Lin, H.J. Liu, K.M. Chen, Utilization of dried activated sludge for the removal of basic dye from aqueous solution, Desal. Wat. Treat., 51 (2013) 7074–7080.

[36] J. Cao, Q. Mao, L. Shi, Y. Qian, Fabrication of γ-MnO_2/α-MnO_2 hollow core/shell structures and their application to water treatment, J. Mater. Chem., 21 (2011) 16210–16215.

[37] W.J. Ji, R.Q. Hao, W.W. Pei, L. Feng, Q.G. Zhai, Design of two isoreticular Cd-biphenyltetracarboxylate frameworks for dye adsorption, separation and photocatalytic degradation, Dalton Trans., 47 (2018) 9226–9234.

[38] N.C. Le, D.V. Phuc, Sorption of lead (II), cobalt (II) and copper (II) ions from aqueous solutions by γ-MnO_2 nanostructure, Adv. Nat. Sci. Nanosci. Nanotechnol., 6 (2015) 025014 (1–8).

[39] P.H. Ho, S.C. Lee, J. Kim, D. Lee, H.C. Woo, Properties of a manganese oxide octahedral molecular sieve (OMS-2) for adsorptive desulfurization of fuel gas for fuel cell applications, Fuel Process. Technol., 131 (2015) 238–246.

[40] X. Li, B. Hu, S. Suib, Y. Lei, B. Li, Manganese dioxide as a new cathode catalyst in microbial fuel cells, J. Power Sources, 195 (2010) 2586–2591.

[41] J.J. Dolhun, Observations on manganese dioxide as a catalyst in the decomposition of hydrogen peroxide: a safer demonstration, J. Chem. Educ., 91 (2014) 760–762.

[42] S.L. Brock, N. Duan, Z.R. Tian, O. Giraldo, H. Zhou, S.L. Suib, A review of porous manganese oxide materials, Chem. Mater., 10 (1998) 2619–2628.
[43] Y. Chen, Y. Hong, Y. Ma, J. Li, Synthesis and formation mechanism of urchin-like nano/micro-hybrid α-mnO_2, J. Alloys Compd., 490 (2010) 331–335.
[44] W. Zhang, Z. Yang, X. Wang, Y. Zhang, X. Wen, S. Yang, Large-scale synthesis of β-MnO_2 nanorods and their rapid and sufficient catalytic oxidation of methylene blue dye, Catal. Commun., 7 (2006) 408–412.
[45] S. Ching, E. J. Welch, S. M. Hughes, A. B. F. Bahadoor, Nonaqueous sol-gel syntheses of microporous manganese oxides, Chem. Mater., 14 (2002) 1292–1299.
[46] S. Nagamuthu, S. Vijayakumar, G. Muralidharan, Synthesis of Mn_3O_4/amorphous carbon nanoparticles as electrode material for high performance supercapacitor applications, Energy Fuels, 27 (2013) 3508–3515.
[47] P. Zhang, D. Sun, M. He, J. Lang, S. Xu, X. Yan, Synthesis of porous δ-MnO_2 submicron tubes as highly efficient electrocatalyst for rechargeable Li-O_2 batteries, ChemSusChem, 8 (2015) 1972–1979.
[48] A.J. Roberts, R.C.T. Slade, Controlled synthesis of ε-MnO_2 and its application in hybrid supercapacitor devices, J. Mater. Chem., 20 (2010) 3221–3226.
[49] G. Xu, Y. Xu, H. Sun, F. Fu, X. Zheng, L. Huang, J. Li, Sh. Yang, S. Sun, Facile synthesis of porous MnO microspheres for high-performance lithium-ion batteries., Part. Part. Syst. Char., 31 (2014) 1001–1007.
[50] B. Yin, S. Zhang, Y. Jiao, Y. Liu, F. Qu, X. Wu, Facile synthesis of ultra-long MnO_2 nanowires as high performance supercapacitor electrodes and photocatalysts with enhanced photocatalytic activities, Cryst. Eng. Comm, 16 (2014) 9999–10005.
[51] S. Jana, S. Pande, A.K. Sinha, S. Sarkar, M. Pradhan, M. Basu, S. Saha, T. Pal, A green chemistry approach for the synthesis of flower-like Ag-doped MnO_2 nanostructures probed by surface-enhanced Raman spectroscopy, J. Phys. Chem. C., 113 (2009) 1386–1392.
[52] J. Fei, Y. Cui, X. Yan, W. Qi, Y. Yang, K. Wang, Q. He, J. Li, Controlled preparation of MnO_2 hierarchical hollow nanostructures and their application in water treatment, Adv. Mater., 2 (2008) 452–456.
[53] Y.C. Zhang, T.Q, X. Ya Hu, W.D. Zhou, Simple hydrothermal preparation of γ-MnOOH nanowires and their low-temperature thermal conversion to β-MnO_2 nanowires, J. Cryst. Growth, 280 (2005) 652–657.
[54] M. Thomas, K. Barbusiński, S. Kliś, E. Szpyrka, M. Chyc, Synthetic textile wastewater treatment using potassium ferrate(VI)–application of Taguchi method for optimization of experiment, Fibers Text. East. Eur., 26 (2018) 104–109.
[55] A. Karimi, F. Mahdizadeh, D. Salari, A. Niaei, Bio-deoxygenation of water using glucose oxidase immobilized in mesoporous MnO_2, Desalination, 275 (2011) 148–153.
[56] D.S. Tong, C. H. Zhou, Y. Lu, H. Yu, G.F. Zhang, W.H. Yu, Adsorption of Acid Red G dye on octadecyl trimethyl ammonium montmorillonite, Appl. Clay Sci., 50 (2010) 427–431.
[57] M. Sun, B. Lan, T. Lin, G. Cheng, F. Ye, L. Yu, X. Cheng, X. Zheng, Controlled synthesis of nanostructured manganese oxide: Crystalline evolution and catalytic activities, CrystEngComm, 15 (2013) 7010–7018.
[58] F. Li, C. Liu, C Liang, X. Li, L. Zhang, The oxidative degradation of 2-mercaptobenzothiazole at the interface of β-MnO_2 and water, J. Hazard. Mater., 154 (2008) 1098–1105.
[59] K.A. Block, A. Trusiak, A. Katz, A. Alimova, H. Wei, P. Gottlieb, J.C. Steiner, Exfoliation and intercalation of montmorillonite by small peptides, Appl. Clay Sci., 107 (2015) 173–181.
[60] S.K. Sharma (Editor), Green chemistry for dyes removal from wastewater, research trends and applications, Wiley–Scrivener Publishing LLC, Salem, MA, 2015.
[61] P.F. Smith, B.J. Deibert, S. Kaushik, G. Gardner, S. Hwang, H. Wang, J.F. Al-Sharab, E. Garfunkel, L. Fabris, J. Li, G.C. Dismukes, Coordination geometry and oxidation state requirements of corner sharing MnO_6 octahedral for water oxidation catalysis: an investigation of manganite (γ-MnOOH), ACS Catal., 6 (2016) 5435–5449.
[62] A. Ubowska, Montmorillonite as a polyurethane foams flame retardant, Arch. Combust., 30 (2010) 459–462.
[63] V.S. Munagapati, V. Yarramuthi, Y. Kim, K.M. Lee, D.S. Kim, Removal of anionic dyes (Reactive Black 5 and Congo Red) from aqueous solutions using banana peel powder as an adsorbent, Ecotox. Environ. Safe. 148 (2018) 601–607.
[64] X. Shen, X. Chen, D. Sun, T. Wu, Y. Li, Fabrication of a magnetite/diazonium functionalized-reduced graphene oxide hybrid as an easily regenerated adsorbent for efficient removal of chlorophenols from aqueous solution, RSC Adv., 99 (2018) 7351–7360.
[65] M. Toor, B. Jin, Adsorption characteristics, isotherm, kinetics, and diffusion of modified natural bentonite for removing diazo dye original research article, Chem. Eng. J., 187 (2012) 79–88.
[66] B. Subramanyam, A. Das, Linearized and non-linearized isotherm models comparative study on adsorption of aqueous phenol solution in soil, Int. J. Environ. Sci. Tech., 6 (2009) 633–640.
[67] S.R. Taffarel, J. Rubio, Removal of Mn^{2+} from aqueous solution by manganese oxide coated zeolite, Miner. Eng., 23 (2010) 1131–1138.
[68] F. Urszula, Adsorption and desorption of reactive dyes onto chitin and chitosan flakes and beads, Adsorpt. Sci. Technol., 24 (2006) 781–796.
[69] B. Balci, F.E. Erkurt, Adsorption of reactive dye from aqueous solution and synthetic dye bath wastewater by eucalyptus bark/magnetite composite, Water Sci. Technol., 74.6 (2016) 1386–1397.
[70] M. Faraji, Y. Yamini, E. Tahmasebi, A. Saleh, F. Nourmohammadian, Cetyltrimethylammonium bromide-coated magnetite nanoparticles as highly efficient adsorbent for rapid removal of reactive dyes from the textile companies' wastewaters, J. Iran. Chem. Soc., 7 (2010) S130–S144.
[71] T. Poursaberi, M. Hassanisadi, Magnetic removal of Reactive Black 5 from wastewater using ionic liquid grafted magnetic nanoparticles, Clean: Soil Air Water, 41 (2013) 1208–1215.
[72] H.D. Choi, M.C. Shin, D.H. Kim, C.S. Jeon, K. Baek, Removal characteristics of Reactive Black 5 using surfactant modified activated carbon, Desalination, 223 (2008) 290–298.
[73] Z. Eren, F. Nuran, Adsorption of Reactive Black 5 from an aqueous solution: equilibrium and kinetic studies, Desalination, 194 (2006) 1–10.
[74] M. Wawrzkiewicz, M. Wisniewska, V.M. Gun'ko, Application of silica–alumina oxides of different compositions for removal of C.I. Reactive Black 5 dye from wastewaters, Adsorpt. Sci. Technol., 35 (2017) 448–457.
[75] T.K. Saha, N.C. Bhoumik, S. Karmaker, M. Ghafari Ahmed, H. Ichikawa, Y. Fukumori, Adsorption characteristics of Reactive Black 5 from aqueous solution onto chitosan, Clean Soil Air Water, 39 (2011) 984–993.
[76] M. Farrokhi, S.C. Hosseini, J.K. Yang, M. ShirzadSiboni, Application of ZnO-Fe_3O_4 nanocomposite on the removal of azo dye from aqueous solutions: kinetics and equilibrium studies, Water Air Soil Pollut., 225: 2113 (2014) 1–12.
[77] B. Heibati, S. Rodriguez-Couto, A. Amrane, M. Rafatullah, A. Hawari, M.A. Al-Ghouti, Uptake of Reactive Black 5 by pumice and walnut activated carbon: chemistry and adsorption mechanisms, J. Ind. Eng. Chem., *20* (2014) *2939–2947.*
[78] D. Karadag, M. Turan, E. Akgul, S. Tok, A. Faki, Adsorption equilibrium and kinetics of Reactive Black 5 and Reactive Red 239 in aqueous solution onto surfactant-modified zeolite, J. Chem. Eng. Data, 52 (2007) 1615–1620.
[79] A. Khan, A. Rashid, R. Younas, Adsorption of Reactive Black-5 by pine needles biochar produced via catalytic and non-catalytic pyrolysis, Arab. J. Sci. Eng., 40 (2015) 1269–1278.